MULTIPLE SCATTERING EFFECTS ON THE LOCALIZATION OF TWO POINT SCATTERERS

Gang Shi[†], Arye Nehorai[‖], Hongwei Liu[§], Bo Chen[§], Yuehai Wang[‡]

[†]State Key Laboratory of Integrated Services Networks, Xidian University
[‖]Green Department of Electrical and Systems Engineering, Washington University in St. Louis
[§]National Lab of Radar Signal Processing, Xidian University
[‡]Institute of Information and Communication Engineering, Zhejiang University

ABSTRACT

Multiple scattering effects are commonly ignored in the detection and estimation of scatterers in signal processing research, because the energy of the first-order scattering is much larger than that of higher-order components. Although multiple scattering can significantly increase the estimation precision of point scatterers, it does not always lead to an improvement. Identifying conditions under which multiple scattering is beneficial or detrimental to estimation in a general setup is still an open problem. In this paper, we consider the effects of multiple scattering on the localization of two point scatterers. By comparing the Fisher information matrix on location parameters when multiple scattering exists and does not exist, we show analytically that information on ranges can benefit estimating directions of arrival via multiple scattering when the two scatterers are in far-field and well resolved.

***Index Terms*—** Multiple Scattering, Fisher Information, Cramér-Rao Bound, Estimation, Artificial Scatterer

1. INTRODUCTION

Single scattering is a usual assumption in sensing signal processing research: The signal observed at the receiver side is assumed to come from a wave that has traveled from a transmitter to a scatterer and then back-scattered to the receiver. When multiple scatterers exist, the received signal is typically modeled as the sum of waves scattered by each individual scatterer. Even though the wave scattered by one scatterer may propagate to other scatterers and arrive at the receiver via multiple paths, such interactions among scatterers due to multiple scattering [1] are largely ignored because the energy of the single scattering, i.e., the first-order scattering, is much larger than that of higher-order components. How multiple scattering affects the precision of estimating scatterers and their imaging resolution has been investigated in a number of studies [2]-[10], but the results are controversial. Shi and Nehorai derived a closed-form physical model to account for multiple scattering [2] and Cramér-Rao bounds (CRBs) [3] on the precision of estimating the location and scattering parameters of point scatterers. By comparing the CRBs for multiple scattering with a reference case that has only single scattering, they showed that multiple scattering could significantly improve the estimation performance. Sentenac et al. investigated the influence of multiple scattering on the CRB for the estimation of the inter-distance between two objects [4], in which they observed that the occurrence of strong multiple scattering does not automatically lead to a resolution enhancement. Chen and Zhong studied the role of multiple scattering in the framework of transverse electric electromagnetic inverse scattering and showed that multiple scattering does not always improve the accuracy of estimation [5]. Simonetti et al. considered the possibility of retrieving the subwavelength structure of an object when it is illuminated and detected in a far-field location [6], [7]. They demonstrated that the imaging resolution can go beyond the diffraction limit by exploring the multiple scattering within the medium. On the other hand, de Rosny and Prada argued that subwavelength detection is still possible even without multiple scattering between the subwavelength structures [8].

Given the inconsistent effects of multiple scattering on the estimation and imaging of scatterers, identifying conditions under which multiple scattering is favorable or detrimental is crucial. Marengo et al. made such an attempt by considering a system of two scatterers with a single transmitter and single receiver [9], [10]. Assuming only one location parameter is unknown and comparing its CRBs under the cases with and without multiple scattering, they identified some sufficient or necessary conditions. Because of the highly non-linear nature of the physical model as well as the CRBs when multiple scattering is incorporated, comparing CRBs analytically in a general setup is challenging and identifying such conditions is still an open problem. In this paper, we consider a system of two point scatterers under a general multistatic configuration with multiple transmitters and multiple receivers. Assuming all location parameters of the scatterers are unknown, we compare analytically the Fisher information matrices (FIMs) when multiple scattering either exists or does not. We show that when the two scatterers are in far-field locations and well resolved [11], multiple scattering is favorable for the estimation.

2. MODELS AND CRAMÉR-RAO BOUNDS

We briefly describe the two physical models employed in this work: One incorporates multiple scattering and the other includes only single scattering. Although the second model is a first-order approximation of the first one, we treat it as if it were exact in the comparisons, i.e., it represents a fictitious reference scenario where there is no multiple scattering among the scatterers. A complete presentation of the two models can be found in [2], and closed-form CRBs for estimating the location and scattering parameters of multiple scatterers were derived in [3].

We consider two point scatterers at unknown positions $\boldsymbol{x}_1$ and $\boldsymbol{x}_2$, where $\boldsymbol{x}_1, \boldsymbol{x}_2 \in \mathbb{R}^3$ and assume that their scattering coefficients τ_1 and τ_2 are known, where τ_1 and τ_2 are complex numbers. A

The work of G. Shi was supported by Xidian University Grant No. 7215616803, the work of A. Nehorai was supported by AFOSR Grant No. FA9550-11-1-0210.

transmit and receive array of N isotropic point antennas is used to illuminate and localize the scatterers, the elements of which are at known positions $\boldsymbol{\alpha}_1, \boldsymbol{\alpha}_2, \ldots, \boldsymbol{\alpha}_N \in \mathbb{R}^3$. See Figure 1 for the multistatic illustration.

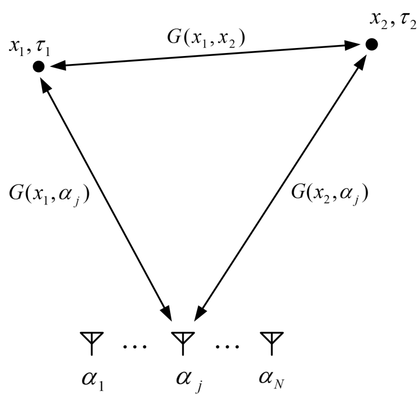

Fig. 1. Illustration of the multistatic setup.

2.1. Model and Cramér-Rao Bound with Multiple Scattering

Using the Foldy-Lax model [12]-[15] as a basis for incorporating multiple scattering, the multistatic response matrix [11] can be formulated in a closed matrix form as [2],

$$K_{\mathrm{FL}} \;=\; A(T^{-1} - S)^{-1} A^T, \tag{1}$$

where $A = [\boldsymbol{g}(\boldsymbol{x}_1), \boldsymbol{g}(\boldsymbol{x}_2)] \in \mathbb{C}^{N\times 2}$, "^{T}" denotes the matrix transpose, $T = \mathrm{diag}\{\tau_1, \tau_2\}$ and the matrix S is defined as

$$S = \begin{bmatrix} 0 & G(\boldsymbol{x}_1, \boldsymbol{x}_2) \\ G(\boldsymbol{x}_1, \boldsymbol{x}_2) & 0 \end{bmatrix} = [\boldsymbol{s}(\boldsymbol{x}_1), \boldsymbol{s}(\boldsymbol{x}_2)].$$

The Green function $G(\boldsymbol{x}_1, \boldsymbol{x}_2) = -e^{ikR}/4\pi R$ in the three-dimensional space represents the "propagator" from location $\boldsymbol{x}_1$ to $\boldsymbol{x}_2$, where k is the background wave number and $R = |\boldsymbol{x}_1 - \boldsymbol{x}_2|$ is the Euclidean distance between the two scatterers. The transmit and receive Green function vectors $\boldsymbol{g}(\boldsymbol{x}_1), \boldsymbol{g}(\boldsymbol{x}_1) \in \mathbb{C}^N$ are

$$\begin{aligned} \boldsymbol{g}(\boldsymbol{x}_1) \;&=\; [G(\boldsymbol{x}_1, \boldsymbol{\alpha}_1), G(\boldsymbol{x}_1, \boldsymbol{\alpha}_2), \ldots, G(\boldsymbol{x}_1, \boldsymbol{\alpha}_N)]^T, \\ \boldsymbol{g}(\boldsymbol{x}_2) \;&=\; [G(\boldsymbol{x}_2, \boldsymbol{\alpha}_1), G(\boldsymbol{x}_2, \boldsymbol{\alpha}_2), \ldots, G(\boldsymbol{x}_2, \boldsymbol{\alpha}_N)]^T, \end{aligned}$$

where $G(\boldsymbol{x}_m, \boldsymbol{\alpha}_j) = -e^{ikR_{m,j}}/4\pi R_{m,j}$ and $R_{m,j} = |\boldsymbol{x}_m - \boldsymbol{\alpha}_j|$ for $m = 1, 2$ and $j = 1, 2, \ldots, N$.

Assume that the measured multistatic response matrix is a noisy version of (1) and the noises are additive, independent, and identically distributed following a multivariate, complex, circularly-symmetric Gaussian distribution. The CRB for estimating the location parameters $\boldsymbol{x} = [\boldsymbol{x}_1^T, \boldsymbol{x}_2^T]^T$ can be computed as the inverse of the FIM

$$\mathcal{I}_{\mathrm{FL}}(\boldsymbol{x}) \;=\; \frac{2}{\sigma^2}\Re\{D_{\mathrm{FL}}^H D_{\mathrm{FL}}\}, \tag{2}$$

where σ^2 is the variance of the noise, $\Re\{\cdot\}$ takes the real part of a complex matrix, and "^{H}" denotes the conjugate transpose, $D_{\mathrm{FL}} = \partial \mathrm{vec}(K_{\mathrm{FL}})/\partial \boldsymbol{x}^T$ and $\mathrm{vec}(\cdot)$ vectorizes a matrix by stacking its columns one under another. The Jacobian matrix D_{FL} was derived in [3] as

$$\begin{aligned} D_{\mathrm{FL}} \;=\; & A(T^{-1} - S)^{-1} \otimes \mathbf{1}_n^T \odot B - [A(T^{-1} - S)^{-1} \otimes \\ & A(T^{-1} - S)^{-1}]C + B \odot [A(T^{-1} - S)^{-1} \otimes \mathbf{1}_n^T], \end{aligned} \tag{3}$$

where "$\otimes$" denotes the Kronecker product [17], $\mathbf{1}_n$ is an n-dimensional column vector with each element as 1, n is the dimension of one location coordinate, for instance $n = 3$ for the three-dimensional formulation, "$\odot$" denotes the Khatri-Rao product [17], $B = [\boldsymbol{b}(\boldsymbol{x}_1), \boldsymbol{b}(\boldsymbol{x}_2)]$, $\boldsymbol{b}(\boldsymbol{x}_m) = \partial \boldsymbol{g}(\boldsymbol{x}_m)/\partial \boldsymbol{x}_m^T$ for $m = 1, 2$ and $C = [\boldsymbol{c}^T(\boldsymbol{x}_1), \boldsymbol{c}^T(\boldsymbol{x}_2)]^T$, $\boldsymbol{c}(\boldsymbol{x}_m) = \partial \boldsymbol{s}(\boldsymbol{x}_m)/\partial \boldsymbol{x}^T$ for $m = 1, 2$.

2.2. Model and Cramér-Rao Bound without Multiple Scattering

We employ the Born-approximated model [12], [16] as the reference model for studying the effect of multiple scattering. In this case, the multistatic response matrix that includes only single scattering is modeled as

$$K_{\mathrm{B}} = ATA^T = \tau_1 \boldsymbol{g}(\boldsymbol{x}_1)\boldsymbol{g}^T(\boldsymbol{x}_1) + \tau_2 \boldsymbol{g}(\boldsymbol{x}_2)\boldsymbol{g}^T(\boldsymbol{x}_2). \tag{4}$$

The corresponding CRB is the inverse of the following FIM

$$\mathcal{I}_{\mathrm{B}}(\boldsymbol{x}) \;=\; \frac{2}{\sigma^2}\Re\{D_{\mathrm{B}}^H D_{\mathrm{B}}\}, \tag{5}$$

where $D_{\mathrm{B}} = \partial \mathrm{vec}(K_{\mathrm{B}})/\partial \boldsymbol{x}^T$. The Jacobian matrix D_{B} is [3]

$$D_{\mathrm{B}} \;=\; AT \otimes \mathbf{1}_n^T \odot B + B \odot (AT \otimes \mathbf{1}_n^T). \tag{6}$$

It is easy to see that K_{B} and D_{B} are special cases of K_{FL} and D_{FL}, respectively, when S is set to be a zero matrix.

3. FISHER INFORMATION MATRIX COMPARISON

Instead of comparing the CRBs for the two cases directly, we compare the corresponding FIMs, because, for two matrices A and B, $A^{-1} \leq B^{-1}$ if and only if $A \geq B$ [18]. Here, $A \geq B$ means that $A - B$ is positive semidefinite. To evaluate the two FIMs $\mathcal{I}_{\mathrm{FL}}(\boldsymbol{x})$ and $\mathcal{I}_{\mathrm{B}}(\boldsymbol{x})$, we first compute matrices B and C in (3) and (6). The derivatives of the Green functions with respect to the location parameters can be calculated as

$$\begin{aligned} \frac{\partial G(\boldsymbol{x}_m, \boldsymbol{\alpha}_j)}{\partial \boldsymbol{x}_m} \;&=\; G(\boldsymbol{x}_m, \boldsymbol{\alpha}_j)\frac{ikR_{m,j} - 1}{R_{m,j}^2}(\boldsymbol{x}_m - \boldsymbol{\alpha}_j) \\ &\approx\; ikG(\boldsymbol{x}_m, \boldsymbol{\alpha}_j)\overrightarrow{\boldsymbol{x}_m - \boldsymbol{\alpha}_j}, \end{aligned}$$

where $\overrightarrow{\boldsymbol{x}_m - \boldsymbol{\alpha}_j} = (\boldsymbol{x}_m - \boldsymbol{\alpha}_j)/R_{m,j}$ for $j = 1, 2, \ldots, N$, $m = 1, 2$, and the approximation holds when $R_{m,j} \gg 1$. Therefore,

$$\begin{aligned} \boldsymbol{b}(\boldsymbol{x}_m) \;&\approx\; ik[G(\boldsymbol{x}_m, \boldsymbol{\alpha}_1)\overrightarrow{\boldsymbol{x}_m - \boldsymbol{\alpha}_1}, \cdots, G(\boldsymbol{x}_m, \boldsymbol{\alpha}_N)\overrightarrow{\boldsymbol{x}_m - \boldsymbol{\alpha}_N}]^T \\ &\approx\; ik\boldsymbol{g}(\boldsymbol{x}_m) \otimes \overrightarrow{\boldsymbol{x}_m - \boldsymbol{\alpha}}^T, \end{aligned} \tag{7}$$

where $\boldsymbol{\alpha}$ is the geometric center of the transmit and receive array. In the second approximation, we use $\overrightarrow{\boldsymbol{x}_m - \boldsymbol{\alpha}_j} \approx \overrightarrow{\boldsymbol{x}_m - \boldsymbol{\alpha}}$ for $j = 1, 2, \ldots, N$ and $m = 1, 2$ assuming that the scatterers are in the far field with respect to the array. This approximation is essentially also a monostatic approximation. Thus, we have

$$B = [\boldsymbol{b}(\boldsymbol{x}_1), \boldsymbol{b}(\boldsymbol{x}_2)] \approx ik[\boldsymbol{g}(\boldsymbol{x}_1) \otimes \overrightarrow{\boldsymbol{x}_1 - \boldsymbol{\alpha}}^T, \boldsymbol{g}(\boldsymbol{x}_2) \otimes \overrightarrow{\boldsymbol{x}_2 - \boldsymbol{\alpha}}^T]. \tag{8}$$

Analogously, when the two scatterers are well separated, i.e., $R \gg 1$, we have

$$\begin{aligned} \partial \boldsymbol{s}(\boldsymbol{x}_1)/\partial \boldsymbol{x}_1^T \;&\approx\; ik\boldsymbol{s}(\boldsymbol{x}_1) \otimes \overrightarrow{\boldsymbol{x}_1 - \boldsymbol{x}_2}^T, \\ \partial \boldsymbol{s}(\boldsymbol{x}_1)/\partial \boldsymbol{x}_2^T \;&\approx\; ik\boldsymbol{s}(\boldsymbol{x}_1) \otimes \overrightarrow{\boldsymbol{x}_2 - \boldsymbol{x}_1}^T, \\ \partial \boldsymbol{s}(\boldsymbol{x}_2)/\partial \boldsymbol{x}_1^T \;&\approx\; ik\boldsymbol{s}(\boldsymbol{x}_2) \otimes \overrightarrow{\boldsymbol{x}_1 - \boldsymbol{x}_2}^T, \\ \partial \boldsymbol{s}(\boldsymbol{x}_2)/\partial \boldsymbol{x}_2^T \;&\approx\; ik\boldsymbol{s}(\boldsymbol{x}_2) \otimes \overrightarrow{\boldsymbol{x}_2 - \boldsymbol{x}_1}^T, \end{aligned}$$

where $\overrightarrow{\boldsymbol{x}_1-\boldsymbol{x}_2} = (\boldsymbol{x}_1-\boldsymbol{x}_2)/R$ and $\overrightarrow{\boldsymbol{x}_2-\boldsymbol{x}_1} = (\boldsymbol{x}_2-\boldsymbol{x}_1)/R$. Then, matrix C can be approximated as

$$\begin{aligned} C &= [\boldsymbol{c}^T(\boldsymbol{x}_1), \boldsymbol{c}^T(\boldsymbol{x}_2)]^T \\ &\approx ik \begin{bmatrix} \boldsymbol{s}(\boldsymbol{x}_1) \otimes \overrightarrow{\boldsymbol{x}_1-\boldsymbol{x}_2}^T, & \boldsymbol{s}(\boldsymbol{x}_1) \otimes \overrightarrow{\boldsymbol{x}_2-\boldsymbol{x}_1}^T \\ \boldsymbol{s}(\boldsymbol{x}_2) \otimes \overrightarrow{\boldsymbol{x}_1-\boldsymbol{x}_2}^T, & \boldsymbol{s}(\boldsymbol{x}_2) \otimes \overrightarrow{\boldsymbol{x}_2-\boldsymbol{x}_1}^T \end{bmatrix} \\ &= ik\mathrm{vec}(S) \otimes [\overrightarrow{\boldsymbol{x}_1-\boldsymbol{x}_2}^T, \overrightarrow{\boldsymbol{x}_2-\boldsymbol{x}_1}^T]. \end{aligned} \tag{9}$$

Substituting (8) and (9) into (3), we have

$$\begin{aligned} &D_{\mathrm{FL}} \approx ik\big[(2\tau_1\boldsymbol{g}_1 \otimes \boldsymbol{g}_1 + \tau_1\tau_2 G\boldsymbol{g}_1 \otimes \boldsymbol{g}_2 + \tau_1\tau_2 G\boldsymbol{g}_2 \otimes \boldsymbol{g}_1) \\ &\otimes \overrightarrow{\boldsymbol{x}_1-\boldsymbol{\alpha}}^T - (\tau_1\tau_2 G\boldsymbol{g}_1 \otimes \boldsymbol{g}_2 + \tau_1\tau_2 G\boldsymbol{g}_2 \otimes \boldsymbol{g}_1) \otimes \overrightarrow{\boldsymbol{x}_1-\boldsymbol{x}_2}^T, \\ &(\tau_1\tau_2 G\boldsymbol{g}_1 \otimes \boldsymbol{g}_2 + \tau_1\tau_2 G\boldsymbol{g}_2 \otimes \boldsymbol{g}_1 + 2\tau_2\boldsymbol{g}_2 \otimes \boldsymbol{g}_2) \otimes \overrightarrow{\boldsymbol{x}_2-\boldsymbol{\alpha}}^T \\ &-(\tau_1\tau_2 G\boldsymbol{g}_1 \otimes \boldsymbol{g}_2 + \tau_1\tau_2 G\boldsymbol{g}_2 \otimes \boldsymbol{g}_1) \otimes \overrightarrow{\boldsymbol{x}_2-\boldsymbol{x}_1}^T\big], \end{aligned} \tag{10}$$

where G, $\boldsymbol{g}_1$ and $\boldsymbol{g}_2$ denote $G(\boldsymbol{x}_1, \boldsymbol{x}_2)$, $\boldsymbol{g}(\boldsymbol{x}_1)$ and $\boldsymbol{g}(\boldsymbol{x}_2)$, respectively. In (10), we ignored the higher-order terms of G and used the approximation

$$\det\big((T^{-1}-S)^{-1}\big) = \frac{1}{1/\tau_1\tau_2 - G^2} \approx \tau_1\tau_2,$$

where $\det(\cdot)$ represents the determinant of a matrix. The approximations hold well when $|G|$ is small, that is, the two scatterers are well separated and the multiple scattering between them is weak. Here, $|\cdot|$ denotes the modulus of a complex number.

The FIM of location parameter $\boldsymbol{x}$ with multiple scattering can be found as

$$\mathcal{I}_{\mathrm{FL}}(\boldsymbol{x}) \approx \frac{2}{\sigma^2}k^2 \begin{bmatrix} E_{\mathrm{FL}1,1} & E_{\mathrm{FL}1,2} \\ E_{\mathrm{FL}2,1} & E_{\mathrm{FL}2,2} \end{bmatrix}, \tag{11}$$

where

$$\begin{aligned} E_{\mathrm{FL}1,1} &= (4|\tau_1|^2||\boldsymbol{g}_1||_{\mathrm{F}}^4 + d)\, \overrightarrow{\boldsymbol{x}_1-\boldsymbol{\alpha}}\, \overrightarrow{\boldsymbol{x}_1-\boldsymbol{\alpha}}^T - d\, \overrightarrow{\boldsymbol{x}_1-\boldsymbol{\alpha}} \\ &\quad \overrightarrow{\boldsymbol{x}_1-\boldsymbol{x}_2}^T - d\, \overrightarrow{\boldsymbol{x}_1-\boldsymbol{x}_2}\, \overrightarrow{\boldsymbol{x}_1-\boldsymbol{\alpha}}^T + d\, \overrightarrow{\boldsymbol{x}_1-\boldsymbol{x}_2}\, \overrightarrow{\boldsymbol{x}_1-\boldsymbol{x}_2}^T \\ E_{\mathrm{FL}1,2} &= d\, \overrightarrow{\boldsymbol{x}_1-\boldsymbol{\alpha}}\, \overrightarrow{\boldsymbol{x}_2-\boldsymbol{\alpha}}^T - d\, \overrightarrow{\boldsymbol{x}_1-\boldsymbol{\alpha}}\, \overrightarrow{\boldsymbol{x}_2-\boldsymbol{x}_1}^T \\ &\quad -d\, \overrightarrow{\boldsymbol{x}_1-\boldsymbol{x}_2}\, \overrightarrow{\boldsymbol{x}_2-\boldsymbol{\alpha}}^T + d\, \overrightarrow{\boldsymbol{x}_1-\boldsymbol{x}_2}\, \overrightarrow{\boldsymbol{x}_2-\boldsymbol{x}_1}^T \\ E_{\mathrm{FL}2,1} &= d\, \overrightarrow{\boldsymbol{x}_2-\boldsymbol{\alpha}}\, \overrightarrow{\boldsymbol{x}_1-\boldsymbol{\alpha}}^T - d\, \overrightarrow{\boldsymbol{x}_2-\boldsymbol{\alpha}}\, \overrightarrow{\boldsymbol{x}_1-\boldsymbol{x}_2}^T \\ &\quad -d\, \overrightarrow{\boldsymbol{x}_2-\boldsymbol{x}_1}\, \overrightarrow{\boldsymbol{x}_1-\boldsymbol{\alpha}}^T + d\, \overrightarrow{\boldsymbol{x}_2-\boldsymbol{x}_1}\, \overrightarrow{\boldsymbol{x}_1-\boldsymbol{x}_2}^T \\ E_{\mathrm{FL}2,2} &= (4|\tau_2|^2||\boldsymbol{g}_2||_{\mathrm{F}}^4 + d)\, \overrightarrow{\boldsymbol{x}_2-\boldsymbol{\alpha}}\, \overrightarrow{\boldsymbol{x}_2-\boldsymbol{\alpha}}^T - d\, \overrightarrow{\boldsymbol{x}_2-\boldsymbol{\alpha}} \\ &\quad \overrightarrow{\boldsymbol{x}_2-\boldsymbol{x}_1}^T - d\, \overrightarrow{\boldsymbol{x}_2-\boldsymbol{x}_1}\, \overrightarrow{\boldsymbol{x}_2-\boldsymbol{\alpha}}^T + d\, \overrightarrow{\boldsymbol{x}_2-\boldsymbol{x}_1} \overrightarrow{\boldsymbol{x}_2-\boldsymbol{x}_1}^T, \end{aligned}$$

$\|\cdot\|_{\mathrm{F}}$ denotes the Frobenius norm of a vector, and

$$d = 2|\tau_1|^2|\tau_2|^2|G|^2||\boldsymbol{g}_1||_{\mathrm{F}}^2||\boldsymbol{g}_2||_{\mathrm{F}}^2.$$

See Appendix A for the proof. When making the approximation in (11), we assumed that the two point scatterers were well-resolved [11], in which case $\boldsymbol{g}_1^H\boldsymbol{g}_2 \approx 0$. From an imaging point of view, well-resolved scatterers correspond to the case where the scatterers are sufficiently separated such that the point spread function of the array does not significantly overlap any scatterer other than the one that it is focused on [11].

For the reference case without multiple scattering, the Jacobian matrix D_{B} and FIM $\mathcal{I}_{\mathrm{B}}(\boldsymbol{x})$ are

$$D_{\mathrm{B}} \approx ik[2\tau_1\boldsymbol{g}_1 \otimes \boldsymbol{g}_1 \otimes \overrightarrow{\boldsymbol{x}_1-\boldsymbol{\alpha}}^T, 2\tau_2\boldsymbol{g}_2 \otimes \boldsymbol{g}_2 \otimes \overrightarrow{\boldsymbol{x}_2-\boldsymbol{\alpha}}^T], \tag{12}$$

$$\mathcal{I}_{\mathrm{B}}(\boldsymbol{x}) \approx \frac{2}{\sigma^2}k^2 \begin{bmatrix} E_{\mathrm{B}1,1} & \mathbf{0} \\ \mathbf{0} & E_{\mathrm{B}2,2} \end{bmatrix}, \tag{13}$$

where

$$\begin{aligned} E_{\mathrm{B}1,1} &= 4|\tau_1|^2||\boldsymbol{g}_1||_{\mathrm{F}}^4\, \overrightarrow{\boldsymbol{x}_1-\boldsymbol{\alpha}}\, \overrightarrow{\boldsymbol{x}_1-\boldsymbol{\alpha}}^T, \\ E_{\mathrm{B}2,2} &= 4|\tau_2|^2||\boldsymbol{g}_2||_{\mathrm{F}}^4\, \overrightarrow{\boldsymbol{x}_2-\boldsymbol{\alpha}}\, \overrightarrow{\boldsymbol{x}_2-\boldsymbol{\alpha}}^T. \end{aligned}$$

It can be verified that (12) and (13) are special cases of (10) and (11), respectively, when G is zero.

The difference between the two FIMs is

$$\Delta\mathcal{I}(\boldsymbol{x}) = \mathcal{I}_{\mathrm{FL}}(\boldsymbol{x}) - \mathcal{I}_{\mathrm{B}}(\boldsymbol{x}) \approx \frac{2}{\sigma^2}k^2 d \begin{bmatrix} E_{\mathrm{I}1,1} & E_{\mathrm{I}1,2} \\ E_{\mathrm{I}2,1} & E_{\mathrm{I}2,2} \end{bmatrix},$$

where

$$\begin{aligned} E_{\mathrm{I}1,1} &= (\overrightarrow{\boldsymbol{x}_1-\boldsymbol{\alpha}} - \overrightarrow{\boldsymbol{x}_1-\boldsymbol{x}_2})(\overrightarrow{\boldsymbol{x}_1-\boldsymbol{\alpha}}^T - \overrightarrow{\boldsymbol{x}_1-\boldsymbol{x}_2}^T), \\ E_{\mathrm{I}1,2} &= (\overrightarrow{\boldsymbol{x}_1-\boldsymbol{\alpha}} - \overrightarrow{\boldsymbol{x}_1-\boldsymbol{x}_2})(\overrightarrow{\boldsymbol{x}_2-\boldsymbol{\alpha}}^T - \overrightarrow{\boldsymbol{x}_2-\boldsymbol{x}_1}^T), \\ E_{\mathrm{I}2,1} &= (\overrightarrow{\boldsymbol{x}_2-\boldsymbol{\alpha}} - \overrightarrow{\boldsymbol{x}_2-\boldsymbol{x}_1})(\overrightarrow{\boldsymbol{x}_1-\boldsymbol{\alpha}}^T - \overrightarrow{\boldsymbol{x}_1-\boldsymbol{x}_2}^T), \\ E_{\mathrm{I}2,2} &= (\overrightarrow{\boldsymbol{x}_2-\boldsymbol{\alpha}} - \overrightarrow{\boldsymbol{x}_2-\boldsymbol{x}_1})(\overrightarrow{\boldsymbol{x}_2-\boldsymbol{\alpha}}^T - \overrightarrow{\boldsymbol{x}_2-\boldsymbol{x}_1}^T). \end{aligned}$$

Let $\boldsymbol{y}_1 = (\overrightarrow{\boldsymbol{x}_1-\boldsymbol{\alpha}}^T, \overrightarrow{\boldsymbol{x}_2-\boldsymbol{\alpha}}^T)^T$, $\boldsymbol{y}_2 = (\overrightarrow{\boldsymbol{x}_1-\boldsymbol{x}_2}^T, \overrightarrow{\boldsymbol{x}_2-\boldsymbol{x}_1}^T)^T$,

$$\begin{aligned} &\Delta\mathcal{I}(\boldsymbol{x}) \\ &\approx \frac{4}{\sigma^2}k^2|\tau_1|^2|\tau_2|^2|G|^2||\boldsymbol{g}_1||_{\mathrm{F}}^2||\boldsymbol{g}_2||_{\mathrm{F}}^2(\boldsymbol{y}_1-\boldsymbol{y}_2)(\boldsymbol{y}_1-\boldsymbol{y}_2)^T, \end{aligned} \tag{14}$$

which is a positive semidefinite matrix. This proves that the FIM with multiple scattering is larger than that without it. The difference (14) represents the gain of Fisher information due to multiple scattering.

4. NUMERICAL EXAMPLE

In order to evaluate the effect of multiple scattering in localizing two well resolved scatterers in far-field, we consider a two-dimensional (2-D) multistatic setup with a numerical example. The analytical results in Section 3 apply without loss of generality. A uniform linear array is used as the transmit and receive array located between (-5,0) and (5,0) with a spacing of 0.5 between adjacent elements, where the coordinates are in the unit of the wavelength. For computing CRBs, we use the following background Green function:

$$G(\boldsymbol{r}, \boldsymbol{r}') = \frac{i}{4}\sqrt{\frac{2}{\pi}}\frac{e^{ik|\boldsymbol{r}-\boldsymbol{r}'|}}{\sqrt{k|\boldsymbol{r}-\boldsymbol{r}'|}}e^{-i\pi/4}, \tag{15}$$

where $\boldsymbol{r}$ and $\boldsymbol{r}'$ are two arbitrary locations. The Green function is a far-field approximation of the zero-order Hankel function of the first kind [19], a solution of the wave equation in the 2-D scenario.

To evaluate the effects of multiple scattering on localizing the two scatterers, we look at $\mathrm{tr}\,\mathrm{CRB}_{\mathrm{B}}(\boldsymbol{x})/\,\mathrm{tr}\,\mathrm{CRB}_{\mathrm{FL}}(\boldsymbol{x})$, the ratio of the traces of the CRBs of the four coordinate parameters based on the Born approximation and the Foldy-Lax model. A ratio larger than one indicates that the sum of lower bounds on the variances of the locations is smaller when multiple scattering exists than that when it does not, i.e., multiple scattering improves the localization of the scatterers. In the numerical example, the two scatterers are located on the line $y = 40$ and are symmetric about the y-axis. The ratio was evaluated with the inter-scatterer spacing varying from 10 to 50, and a total of 101 evaluations were carried out. Although the two scatterers are fixed on line $y = 40$, all location parameters are treated as being unknown and CRBs are computed for all location parameters of the two scatterers. When evaluating the CRBs, all approximations and assumptions employed in Section 3 for analytical comparisons are not used; numerical results are computed in exact forms under the general multistatic configuration.

Simulation results are shown in Figure 2. The upper panel shows the results when $\tau_1 = \tau_2 = 1$. We can see that the precision of localization is generally better with multiple scattering than that without it. The ratio ranges from 0.99 to 1.17 and 99 of the 101 evaluations have a ratio larger than one. The ratio tends to be smaller when the spacing between the scatterers increases. This is because the Fisher information gain (14) due to the multiple scattering is proportional to $|G|^2$, which becomes smaller with increasing inter-scatterer distance. The lower panel displays results for $\tau_1 = 1$, $\tau_2 = 10$. The ratio varies from 3.74 to 11.19 and all of the 101 evaluations demonstrate the enhancement of localization. As in the upper panel, the ratio becomes smaller when the distance between the two scatterers increases.

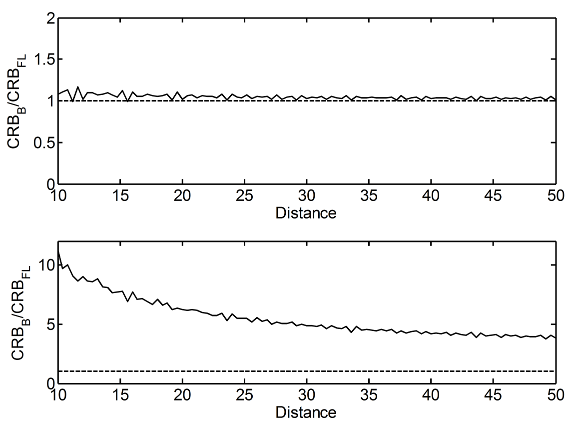

Fig. 2. $\operatorname{tr}\mathrm{CRB}_{\mathrm{B}}(\boldsymbol{x})/\operatorname{tr}\mathrm{CRB}_{\mathrm{FL}}(\boldsymbol{x})$ as a function of the distance between the two scatterers. Upper panel: $\tau_1 = \tau_2 = 1$; lower panel: $\tau_1 = 1, \tau_2 = 10$.

5. DISCUSSION

We proved analytically that multiple scattering is beneficial for estimating the locations of two well-resolved point scatterers in far-field locations. Because the Fisher information gain is proportional to $|G|^2$, the improvement due to the natural multiple scattering that occurs between scatterers could be trivial, at least for well-resolved scatterers, as we illustrated in the upper panel of Figure 2. However, artificial multiple scattering can be introduced to improve the estimation performance in a controlled manner. We proposed the use of the artificial scatterer to improve the performance of multiple-input multiple-output wireless communication systems [20] and to create artificial multiple scattering for improving the estimation of scatterers [3]. In this paper, we illustrated this idea in the lower panel of Figure 2. The scatterer with a scattering coefficient larger than one represents an active artificial scatterer, which receives, amplifies, and transmits back its received wave. As a result, the strength of multiple scattering between the scatterers is larger than what is possible between two passive ones, and the improvement in localization is also much larger.

In Section 3, we made approximation (7) for far-field scatterers. It also ignores phase differences of the received signals at array elements, hence is essentially a monostatic approximation as well. As a result, FIM (13) has a rank of two. It is easy to show in polar coordinates that only ranges of the two scatterers are identifiable. However, if the two scatterers are not located in the same direction, i.e., $\overrightarrow{\boldsymbol{x}_1-\boldsymbol{\alpha}} \neq \overrightarrow{\boldsymbol{x}_2-\boldsymbol{\alpha}}$, the FIM (11) will have a rank of four, thanks to the Fisher information gain (14) provided by multiple scattering. This indicates that additional information on directions of arrival can be obtained from the information on ranges via the interaction between the two scatterers. Because of the monostatic approximation (7) we employed in this paper, it represents only part of the multiple scattering effect on the estimation of directions of arrival.

6. CONCLUSIONS

We compared analytically the FIMs for estimating locations of two point scatterers when multiple scattering exists and does not exist. We showed that multiple scattering improves the estimation of directions of arrival when the two scatterers are in far-field and well resolved. When natural multiple scattering is weak, an artificial scatterer can be introduced to enhance the system performance. Whether or not information on directions of arrival can help estimating ranges with the existence of multiple scattering is worthy of further investigation.

7. APPENDIX A: PROOF OF (11)

$$
\begin{aligned}
&D_{\mathrm{FL}}^H D_{\mathrm{FL}} \approx k^2 \big[(2\tau_1^* \boldsymbol{g}_1^H \otimes \boldsymbol{g}_1^H + \tau_1^*\tau_2^* G^* \boldsymbol{g}_1^H \otimes \boldsymbol{g}_2^H + \\
&\tau_1^*\tau_2^* G^* \boldsymbol{g}_2^H \otimes \boldsymbol{g}_1^H) \otimes \overrightarrow{\boldsymbol{x}_1-\boldsymbol{\alpha}} - (\tau_1^*\tau_2^* G^* \boldsymbol{g}_1^H \otimes \boldsymbol{g}_2^H + \\
&\tau_1^*\tau_2^* G \boldsymbol{g}_2^H \otimes \boldsymbol{g}_1^H) \otimes \overrightarrow{\boldsymbol{x}_1-\boldsymbol{x}_2}, (\tau_1^*\tau_2^* G^* \boldsymbol{g}_1^H \otimes \boldsymbol{g}_2^H + \\
&\tau_1^*\tau_2^* G^* \boldsymbol{g}_2^H \otimes \boldsymbol{g}_1^H + 2\tau_2^* \boldsymbol{g}_2^H \otimes \boldsymbol{g}_2^H) \otimes \overrightarrow{\boldsymbol{x}_2-\boldsymbol{\alpha}} \\
&-(\tau_1^*\tau_2^* G^* \boldsymbol{g}_1^H \otimes \boldsymbol{g}_2^H + \tau_1^*\tau_2^* G^* \boldsymbol{g}_2^H \otimes \boldsymbol{g}_1^H) \otimes \overrightarrow{\boldsymbol{x}_2-\boldsymbol{x}_1}\big] \times \\
&\big[(2\tau_1 \boldsymbol{g}_1 \otimes \boldsymbol{g}_1 + \tau_1\tau_2 G \boldsymbol{g}_1 \otimes \boldsymbol{g}_2 + \tau_1\tau_2 G \boldsymbol{g}_2 \otimes \boldsymbol{g}_1) \otimes \overrightarrow{\boldsymbol{x}_1-\boldsymbol{\alpha}}^T \\
&-(\tau_1\tau_2 G \boldsymbol{g}_1 \otimes \boldsymbol{g}_2 + \tau_1\tau_2 G \boldsymbol{g}_2 \otimes \boldsymbol{g}_1) \otimes \overrightarrow{\boldsymbol{x}_1-\boldsymbol{x}_2}^T, \\
&(\tau_1\tau_2 G \boldsymbol{g}_1 \otimes \boldsymbol{g}_2 + \tau_1\tau_2 G \boldsymbol{g}_2 \otimes \boldsymbol{g}_1 + 2\tau_2 \boldsymbol{g}_2 \otimes \boldsymbol{g}_2) \otimes \overrightarrow{\boldsymbol{x}_2-\boldsymbol{\alpha}}^T \\
&-(\tau_1\tau_2 G \boldsymbol{g}_1 \otimes \boldsymbol{g}_2 + \tau_1\tau_2 G \boldsymbol{g}_2 \otimes \boldsymbol{g}_1) \otimes \overrightarrow{\boldsymbol{x}_2-\boldsymbol{x}_1}^T\big] \\
&\approx k^2 \begin{bmatrix} E_{\mathrm{FL}1,1} & E_{\mathrm{FL}1,2} \\ E_{\mathrm{FL}2,1} & E_{\mathrm{FL}2,2} \end{bmatrix},
\end{aligned}
$$

where

$$
\begin{aligned}
&E_{\mathrm{FL}1,1} \approx \big[(2\tau_1^* \boldsymbol{g}_1^H \otimes \boldsymbol{g}_1^H + \tau_1^*\tau_2^* G^* \boldsymbol{g}_1^H \otimes \boldsymbol{g}_2^H + \tau_1^*\tau_2^* G^* \boldsymbol{g}_2^H \otimes \boldsymbol{g}_1^H) \\
&\otimes \overrightarrow{\boldsymbol{x}_1-\boldsymbol{\alpha}} - (\tau_1^*\tau_2^* G^* \boldsymbol{g}_1^H \otimes \boldsymbol{g}_2^H + \tau_1^*\tau_2^* G^* \boldsymbol{g}_2^H \otimes \boldsymbol{g}_1^H) \otimes \overrightarrow{\boldsymbol{x}_1-\boldsymbol{x}_2}\big] \\
&\big[(2\tau_1 \boldsymbol{g}_1 \otimes \boldsymbol{g}_1 + \tau_1\tau_2 G \boldsymbol{g}_1 \otimes \boldsymbol{g}_2 + \tau_1\tau_2 G \boldsymbol{g}_2 \otimes \boldsymbol{g}_1) \otimes \overrightarrow{\boldsymbol{x}_1-\boldsymbol{\alpha}}^T \\
&-(\tau_1\tau_2 G \boldsymbol{g}_1 \otimes \boldsymbol{g}_2 + \tau_1\tau_2 G \boldsymbol{g}_2 \otimes \boldsymbol{g}_1) \otimes \overrightarrow{\boldsymbol{x}_1-\boldsymbol{x}_2}^T\big] \\
&\approx (4|\tau_1|^2 ||\boldsymbol{g}_1||_{\mathrm{F}}^4 + 2|\tau_1|^2|\tau_2|^2|G|^2||\boldsymbol{g}_1||_{\mathrm{F}}^2||\boldsymbol{g}_2||_{\mathrm{F}}^2) \overrightarrow{\boldsymbol{x}_1-\boldsymbol{\alpha}} \otimes \overrightarrow{\boldsymbol{x}_1-\boldsymbol{\alpha}}^T \\
&-(2|\tau_1|^2|\tau_2|^2|G|^2||\boldsymbol{g}_1||_{\mathrm{F}}^2||\boldsymbol{g}_2||_{\mathrm{F}}^2) \overrightarrow{\boldsymbol{x}_1-\boldsymbol{\alpha}} \otimes \overrightarrow{\boldsymbol{x}_1-\boldsymbol{x}_2}^T \\
&-(2|\tau_1|^2|\tau_2|^2|G|^2||\boldsymbol{g}_1||_{\mathrm{F}}^2||\boldsymbol{g}_2||_{\mathrm{F}}^2) \overrightarrow{\boldsymbol{x}_1-\boldsymbol{x}_2} \otimes \overrightarrow{\boldsymbol{x}_1-\boldsymbol{\alpha}}^T \\
&+(2|\tau_1|^2|\tau_2|^2|G|^2||\boldsymbol{g}_1||_{\mathrm{F}}^2||\boldsymbol{g}_2||_{\mathrm{F}}^2) \overrightarrow{\boldsymbol{x}_1-\boldsymbol{x}_2} \otimes \overrightarrow{\boldsymbol{x}_1-\boldsymbol{x}_2}^T \\
&= (4|\tau_1|^2 ||\boldsymbol{g}_1||_{\mathrm{F}}^4 + d)\, \overrightarrow{\boldsymbol{x}_1-\boldsymbol{\alpha}}\, \overrightarrow{\boldsymbol{x}_1-\boldsymbol{\alpha}}^T - d\, \overrightarrow{\boldsymbol{x}_1-\boldsymbol{\alpha}}\, \overrightarrow{\boldsymbol{x}_1-\boldsymbol{x}_2}^T \\
&-d\, \overrightarrow{\boldsymbol{x}_1-\boldsymbol{x}_2}\, \overrightarrow{\boldsymbol{x}_1-\boldsymbol{\alpha}}^T + d\, \overrightarrow{\boldsymbol{x}_1-\boldsymbol{x}_2}\, \overrightarrow{\boldsymbol{x}_1-\boldsymbol{x}_2}^T.
\end{aligned}
$$

In the second approximation, we used $(A \otimes B \otimes C)(D \otimes E \otimes F) = AD \otimes BE \otimes CF$ [17] and assumed that the two scatterers are well resolved [11], in which case $\boldsymbol{g}_1^H \boldsymbol{g}_2 \approx 0$. $E_{\mathrm{FL}1,2}$, $E_{\mathrm{FL}2,1}$ and $E_{\mathrm{FL}2,2}$ can be derived analogously. $\square$

8. REFERENCES

[1] A. Battaglia, S. Tanelli, S. Kobayashi, D. Zrnic, R. J. Hogan, C. Simmer, "Multiple-scattering in radar systems: A review," *J Quant Spectrosc Ra,* vol. 111, no. 6, pp. 917-947, 2010.

[2] G. Shi, A. Nehorai, "Maximum likelihood estimation of point scatterers for computational time-reversal imaging," *Commun Inform Syst,* vol. 5, no. 2, pp. 227-256, 2005.

[3] G. Shi, A. Nehorai, "Cramér-Rao bound analysis on multiple scattering in multistatic point-scatterer estimation," *IEEE Trans Signal Proces,* vol. 55, no. 6, pp. 2840-2850, 2007.

[4] A. Sentenac, G. Charles-Antoine, C. C. Patrick, F. Drsek, H. Giovannini, N. Bertaux, "Influence of multiple scattering on the resolution of an imaging system: a Cramér-Rao analysis," *Opt Express,* vol. 15, no. 3, pp. 1340-1347, 2007.

[5] X. Chen, Y. Zhong, "Influence of multiple scattering on subwavelength imaging: transverse electric case," *J Opt Soc Am A,* vol. 27, no. 2, pp. 245-250, 2010.

[6] F. Simonetti, "Multiple scattering: The key to unravel the subwavelength world from the far-field pattern of a scattered wave," *Phys Rev E,* vol. 73, no. 3, Article ID 036619, 2006.

[7] F. Simonetti, M. Fleming, E. A. Marengo, "Illustration of the role of multiple scattering in subwavelength imaging from farfield measurements," *J Opt Soc Am A,* vol. 25, no. 2, pp. 292-303, 2008.

[8] J. de Rosny, C. Prada, "Comment on "Multiple scattering: The key to unravel the subwavelength world from the far-field pattern of a scattered wave," *Phys Rev E,* vol. 75, no. 4, Article ID 048601, 2007.

[9] E. A. Marengo, M. Zambrano-Nunez, P. Berestesky, "Cramér-Rao bound study of multiple scattering effects in target localization," *Int J Antenn Propag,* Article ID 390312, 2012.

[10] E. A. Marengo, P. Berestesky, "Cramér-Rao bound study of multiple scattering effects in target separation estimation," *Int J Antenn Propag,* Article ID 572923, 2013.

[11] A. J. Devaney, "Time reversal imaging of obscured targets from multistatic data," *IEEE Trans Antenn Propag,* vol. 53, no. 5, pp. 1600-1610, 2005.

[12] J. H. Taylor, "Scattering Theory," New York, Wiley, 1972.

[13] L. L. Foldy, "The multiple scattering of waves," *Phys Rev,* vol. 67, pp. 107-119, 1945.

[14] M. Lax, "Multiple scattering of waves," *Rev Mod Phys,* vol. 23, pp. 287-310, 1951.

[15] M. Lax, "Multiple scattering of waves. II. The effective field in dense systems," *Phys Rev,* vol. 85, pp. 621-629, 1952.

[16] R. G. Newton, "Scattering Theory of Waves and Particles," New York, McGraw-Hill, 1966.

[17] J. W. Brewer, "Kronecker products and matrix calculus in system theory," *IEEE Trans Circuits Syst,* vol. cas-25, no. 9, pp. 772-781, 1978.

[18] R. A. Horn, C. R. Johnson, "Matrix Analysis," New York, Cambridge University Press, 2nd edition, 2012.

[19] P. Sheng, "Introduction to Wave Scattering, Localization, and Mesoscopic Phenomena," San Diego, Academic Press, Inc., 1995.

[20] G. Shi, A. Nehorai, "Macrocell multiple-input multiple-output system analysis," *IEEE Trans Wirel Commun,* vol. 5, no. 5, pp. 1076-1085.